Journal of Sound and Vibration (1998) **215**(2), 251–272
Article No. sv981611

DYNAMIC ANALYSIS OF SINGLE-ANCHOR INFLATABLE DAMS

G. V. Mysore and S. I. Liapis

Department of Aerospace and Ocean Engineering, Virginia Polytechnic Institute and State University, Blacksburg, VA 24061-0203, *U.S.A.*

AND

R. H. Plaut

The Charles E. Via Jr Department of Civil Engineering, Virginia Polytechnic Institute and State University, Blacksburg, VA 24061-0105, *U.S.A.*

(*Received* 12 *May* 1997, *and in final form* 4 *March* 1998)

Inflatable dams are flexible, cylindrical structures anchored to a foundation. The three-dimensional vibrational behavior of single-anchor inflatable dams with fins is analyzed, both in the absence of water and in the presence of stationary or parallel flowing water. The dam is modelled as an elastic shell inflated with air and resting on a rigid foundation. The internal pressure is increased slowly until it reaches the desired value. Then the external water is applied and the equilibrium configuration is obtained. Small vibrations about this configuration are considered. The external water is assumed to be inviscid and incompressible, and potential theory is used. The infinite-frequency limit is assumed on the free surface. A boundary element technique is utilized to determine the behavior of the water, and the finite element method is applied to model the structure. Vibration frequencies and mode shapes are computed. The effects of the internal pressure, external water head, and parallel flow velocity on the vibrations of the dam are investigated, and the results are compared to those for the dam in the absence of external water.

1. INTRODUCTION

Inflatable dams are flexible structures attached to a rigid base. They were initially developed by N. M. Imbertson of the Los Angeles Department of Water and Power in the 1950s [1]. Since then, over 2000 inflatable dams have been constructed. A review of published work involving such dams is given in reference [2], and additional publications include references [3–18]. A recent project in Arizona is described on the internet at http://www.tempe.gov/rio/dams.htm.

Most inflatable dams are made of a nylon-reinforced polymer. Their heights range up to 6 m and their lengths may reach 150 m. They are usually inflated with air, but can also be filled with water or a combination of air and water. Inflatable dams have been utilized to divert water for irrigation [18] or groundwater recharging [12], impound water for recreational purposes, raise the height of existing dams, prevent beach erosion, control water flow for hydroelectric production [16], and mitigate flooding by allowing excess water to flow over the deflated dam [18]. They have the potential to be used as temporary dikes or levees to protect buildings and metropolitan areas from flood waters. Although many of these dams are permanently inflated, they have the advantage that they can be

0022–460X/98/320251 + 22 $30.00/0

deflated and lie flat when not needed, and then inflated in a short period of time when required.

Early inflatable dams were anchored along two generators. The vibrations of such double-anchor dams were analyzed in references [2, 14, 17]. Hsieh and Plaut [2] modelled the dam as a long cylindrical membrane and carried out a two-dimensional analysis. The dam was filled with water, and external water was impounded (i.e. held back) on one side. It was assumed that the water was incompressible and inviscid, with hydrodynamic pressures acting on the membrane in the normal direction. The weight of the membrane was neglected in the determination of the equilibrium shape, membrane extensibility was not included, and the influence of damping was ignored. Modes and frequencies of small, free vibrations were determined. The effects of the membrane density, upstream head, and internal head on the vibration frequencies were examined.

Dakshina Moorthy *et al*. [14] investigated three-dimensional vibrations of an inflatable dam impounding water. The dam was modelled as a shell with internal air pressure, and the finite element method was applied to both the structure and the external water. Several water depths were considered. The equilibrium shape of the dam was computed first, and then small vibrations about this shape were analyzed. The effect of the water depth on the vibration frequencies and modes was studied.

Steady-state overflow of an inflatable dam was treated by Wu and Plaut [17]. The dam was assumed to be an inextensible air-inflated membrane. The fluid flow was assumed to be incompressible, inviscid, and irrotational, with specified total upstream head. First the steady-state shapes of the dam and the free surface of the water were computed. Then linear vibrations of the structure about its steady-state configuration were analyzed. As in reference [2], the dam was discretized using the finite difference method, whereas the boundary element method was applied to the fluid. Frequencies and modes were obtained, and the effects of the dam density and damping were investigated.

Most recently-built inflatable dams utilize a single-anchor system, rather than a double-anchor one. The dynamic behavior of such dams has not been analyzed previously, and is the subject of the present paper. In a common type of construction, a thick sheet of reinforced rubber is slit into two sheets of half the thickness, except for a strip near one edge. Then the top and bottom sheets at the opposite edge are clamped to the foundation, and the side edges are sealed. Air is pumped between the two sheets, and the

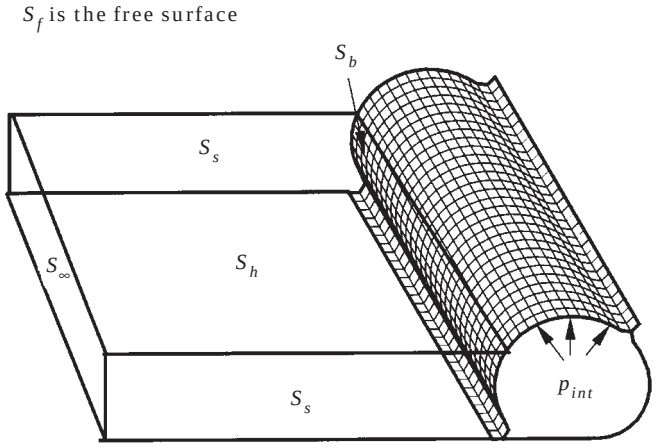

Figure 1. Schematic diagram illustrating the boundary value domain.

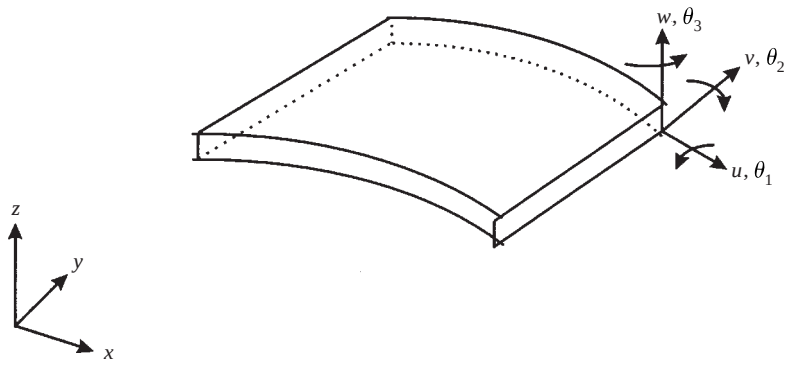

Figure 2. A shell finite element.

upper sheet and part of the lower sheet raise off the foundation. The raised edge that was not slit looks like a fin, as shown in Figure 1.

The inflated dam is modelled as a shell in this study. The finite element method is used to discretize the dam, and the boundary element method is applied to the fluid. The vibrations of the dam in the presence of both external stationary water and parallel flow are considered. Vibrations of shells in contact with external water have been investigated extensively for other geometrical configurations (e.g. cylindrical and spherical shells). References [19–21] are a few of those works. Papers utilizing the finite element method for the structure and the boundary element method for the fluid include references [22, 23] and others listed in reference [24].

The paper is organized as follows. In section 2, model information and procedures for obtaining equilibrium configurations are discussed. In section 3, the linear vibration problem is formulated and the expression for the added mass matrix is derived. Vibration results for the first four modes are presented and discussed in section 4, and concluding remarks are given in section 5.

2. EQUILIBRIUM SHAPES

The dam is modelled as a thin, isotropic, elastic shell and is analyzed using the finite element method. The finite element package ABAQUS is used for performing the static and dynamic analysis. A four-node shell element (the S4R element in ABAQUS [25]) is adopted, which has been developed under the assumptions of large deflections, large rotations, and small strains. Each node of the element has six generalized displacements, u, v, w, θ_1, θ_2, θ_3, with a total of 24 degrees of freedom per element (Figure 2). The surface on which the dam rests is modelled as a rigid surface. A four-node rigid element (the R3D4 element in ABAQUS) is used to model the surface. The boundary conditions are such that there are no deflections or rotations at the anchor line and at the rigid surface.

The equilibrium shapes are obtained numerically. ABAQUS uses Newton's method as a numerical technique for solving the nonlinear equilibrium equations [25]. The basic idea is to reduce the set of nonlinear equations into a set of linear equations by choosing to solve the equilibrium equations at "small" increments, the size of which depends upon the non-linearity of the problem.

The dam is assumed to have negligible weight and a constant internal pressure. External fluid on one side of the dam exerts hydrostatic pressure (Figure 1). Initially, the dam is

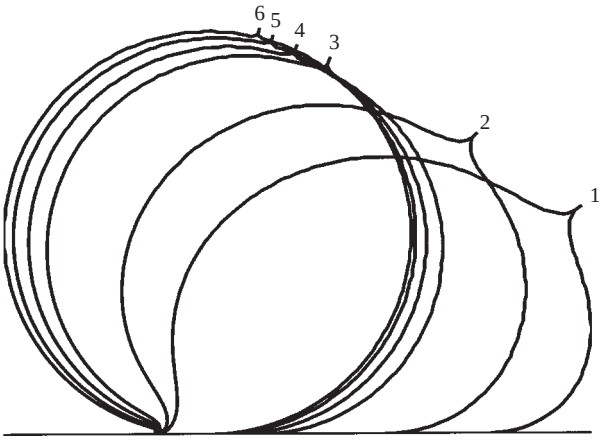

Figure 3. Cross-sectional equilibrium shapes of the dam (at the center) without external water at different internal pressures. (1) $p_{int} = 0{\cdot}5$ kPa; (2) $p_{int} = 1{\cdot}0$ kPa; (3) $p_{int} = 5{\cdot}0$ kPa; (4) $p_{int} = 10$ kPa; (5) $p_{int} = 20$ kPa; (6) $p_{int} = 30$ kPa.

assumed to lie flat. The internal pressure is then gradually increased until it has the desired value. Then the ends are fixed and the external fluid is added at the anchored side of the dam, with its height less than the "dry" equilibrium height of the dam. The density of the fluid is gradually increased from zero to the density of the water (1000 kg/m^3), and the equilibrium shape is obtained.

The finite-length dam is modelled using 1500 elements, with 50 circumferential elements. For all the numerical examples in this paper, the modulus of elasticity of the dam is 0·1038 GPa, the density is 1005 kg/m^3, Poisson's ratio is 0·3, the thickness is 12·7 mm, the dam length is 30 m, and the cross-sectional perimeter is 9·14 m. The internal pressures are

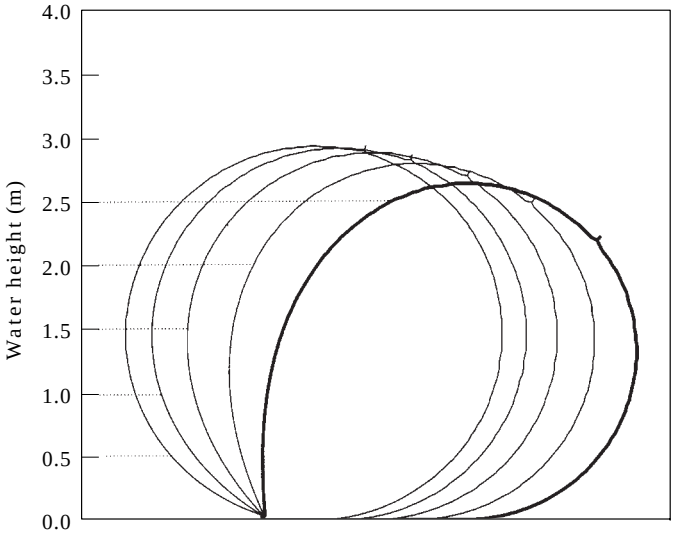

Figure 4. Cross-sectional equilibrium shapes of the dam (at the center) with different water levels, for $p_{int} = 30$ kPa.

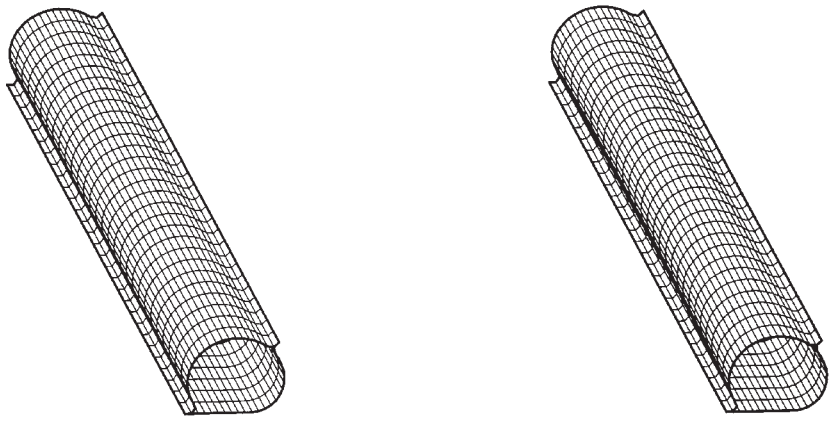

(a) (b)

Figure 5. Equilibrium shapes of the dam, (a) without water, (b) with water, for $p_{int} = 1$ kPa.

varied between 0·5 kPa and 30 kPa. Figure 3 shows the cross-sectional equilibrium shapes at the center of the dam without external water, at different internal pressures. The change in the equilibrium shape with internal pressure is more pronounced for the lower pressures (i.e. from 0·5 kPa to 5 kPa) while the shape tends to become almost circular as the internal pressure is increased. Figure 4 depicts the change in the cross-sectional equilibrium shape at the center of the dam with increasing water level, for an internal pressure of 30 kPa. Figures 5 and 6 illustrate the three-dimensional equilibrium shapes of the dam without and with external water for internal pressures of 1 kPa and 30 kPa, respectively. In Figures 5(a) and 6(a) the height of the center of the dam is 2·4 m and 3·0 m, respectively, and in Figures 5(b) and 6(b) the height of the external water is 0·5 m and 1·5 m, respectively. The external water tends to push the dam towards the right.

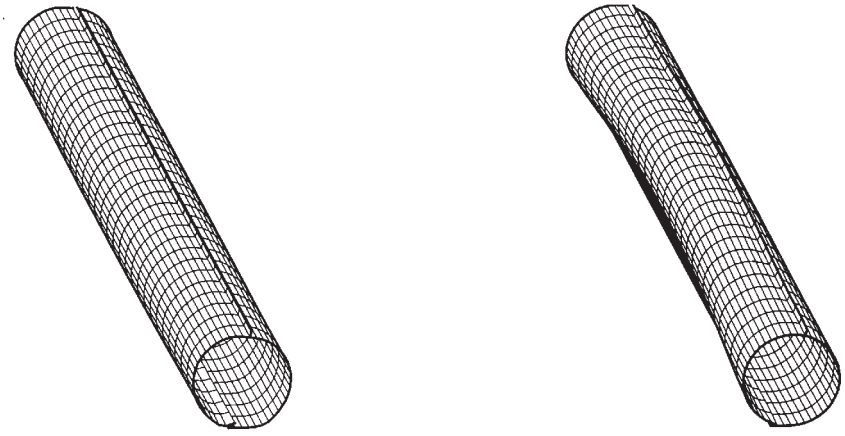

(a) (b)

Figure 6. Equilibrium shapes of the dam, (a) without water, (b) with water, for $p_{int} = 30$ kPa.

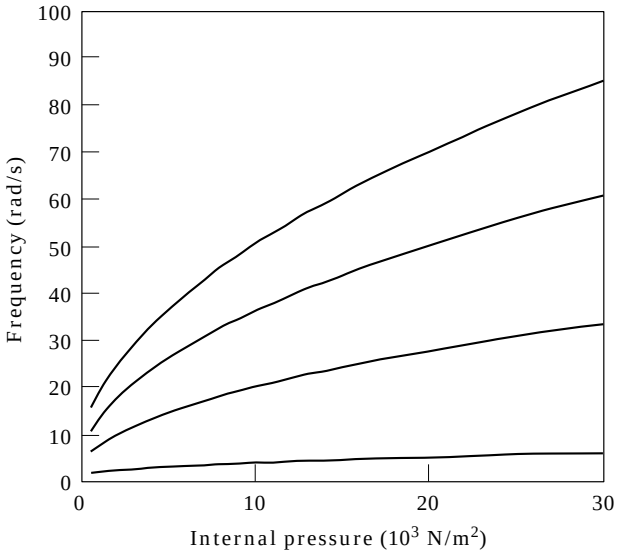

Figure 7. Variation of frequencies with internal pressure, without water.

3. LINEAR VIBRATIONS: FORMULATION

3.1. WITHOUT EXTERNAL WATER

The matrix equation of motion of an inflated dam for small motions about its equilibrium position has the form

$$M\ddot{U} + KU = 0, \tag{1}$$

where U represents the vector of global nodal displacements and M and K are the global mass and stiffness matrices, respectively, of the dam at its equilibrium position. All the matrices in equation (1) are real and symmetric. Standard procedures are used by ABAQUS to obtain the eigenvalues and eigenvectors for simple harmonic motion, and hence the vibration frequencies and modes.

3.2. WITH EXTERNAL WATER

In this case, the matrix equation of the dam for small motions about its equilibrium position takes the form

$$M\ddot{U} + KU = R, \tag{2}$$

TABLE 1

Natural frequencies (rad/s) of the inflatable dam

	$p_{int} = 1$ kPa			$p_{int} = 30$ kPa		
Mode no.	Without water	With hydrostatic pressure	With water	Without water	With hydrostatic pressure	With water
1	2·169	2·512	2·108	5·943	7·151	6·310
2	7·775	8·785	7·401	33·32	38·58	30·87
3	13·49	14·71	12·42	60·67	67·27	53·82
4	19·14	20·91	17·43	84·91	92·66	74·12

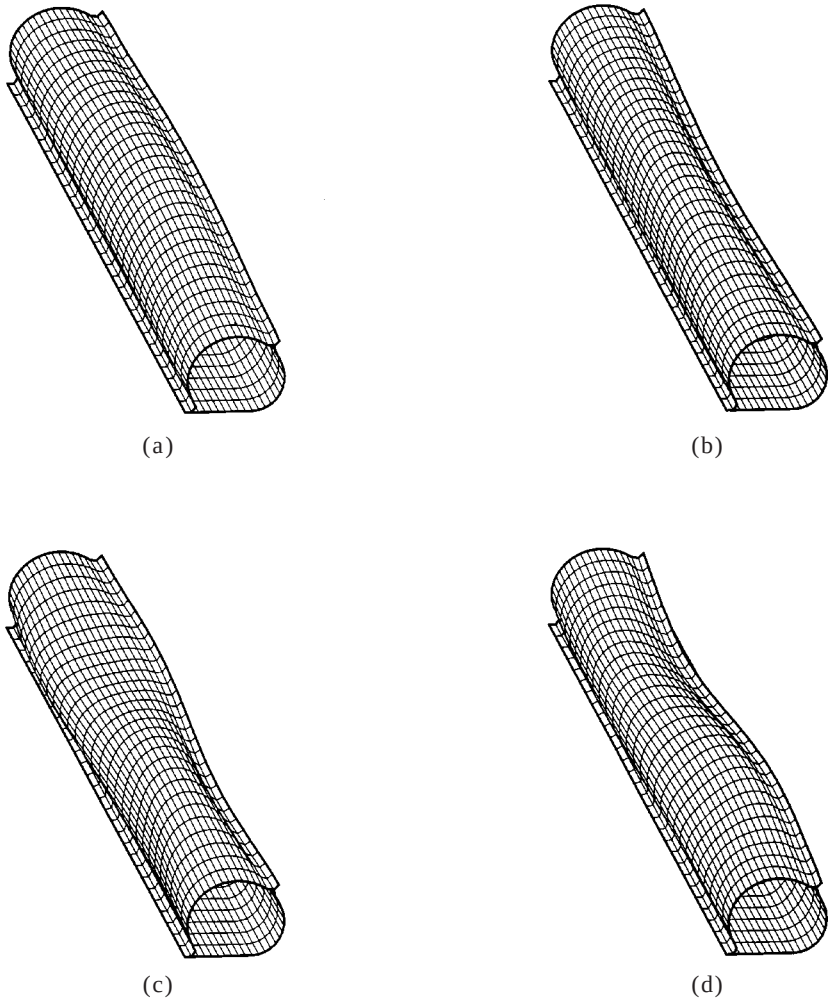

Figure 8. First four vibration modes without external water, for $p_{\text{int}} = 1$ kPa. (a) Mode 1; (b) mode 2; (c) mode 3; (d) mode 4.

where R is the global force vector acting on the dam due to p, which is the change in total pressure of the water due to small motions of the dam about its equilibrium position and due to the external flow of water, with velocity U_p, parallel to the dam. The fluid flow is assumed to be inviscid and irrotational and the fluid is assumed to be incompressible so that the fluid velocities are given by $\mathbf{V} = \nabla\phi$ where ϕ is a velocity potential. Equation (2) defines a typical fluid–structure interaction problem. Several approaches have been proposed to solve such problems. In the present study, we use the "dry" mode shape functions $\psi_j(\mathbf{x})$ [mode shapes obtained after considering the hydrostatic pressure effects but not the dynamic effects of the water (e.g. added mass)] as a basis to define the "wet" modes. Here, $\mathbf{x} = (x, y, z)$. Let $\psi_j(\mathbf{x})$ have Cartesian components (u_j, v_j, w_j). Then the displacement of an arbitrary point on the surface of the dam, due to the corresponding mode, can be written as $\xi_j(t)\psi_j(\mathbf{x})$ where $\xi_j(t)$ is the time-dependent amplitude for mode j. The body surface region S_b is defined as that part of the structure in contact with the external

hydrostatic water (Figure 1). The normal component of $\psi_j(\mathbf{x})$ on S_b is expressed in the form [26]

$$n_j = \psi_j \cdot \mathbf{n} = u_j n_x + v_j n_y + w_j n_z. \tag{3}$$

The unit normal vector $\mathbf{n}$ points out of the fluid domain and into the body. Corresponding to these modes of motion, the generalized pressure forces are defined in the form [26]

$$R_j = \int\int_{S_b} p n_j \, \mathrm{d}S. \tag{4}$$

In the present analysis, wave and structural damping effects are neglected, and only the added mass effect is considered. In order to determine the added mass, we need to determine the fluid motion associated with the vibration of the structure. An xyz coordinate frame is used, with the z axis pointing vertically upwards and the xy plane coinciding with the undisturbed free surface. We denote the wetted surface of the structure by S_b and the fluid domain by D. We assume that the fluid is bounded by S_b, the bottom S_h, the free surface S_f, two side surfaces S_s, and a surface S_∞ far away from the structure (Figure 1). The distance from S_∞ to the structure is taken to be approximately 40 m. It was found that for this distance the boundary condition on S_∞ does not influence the numerical results.

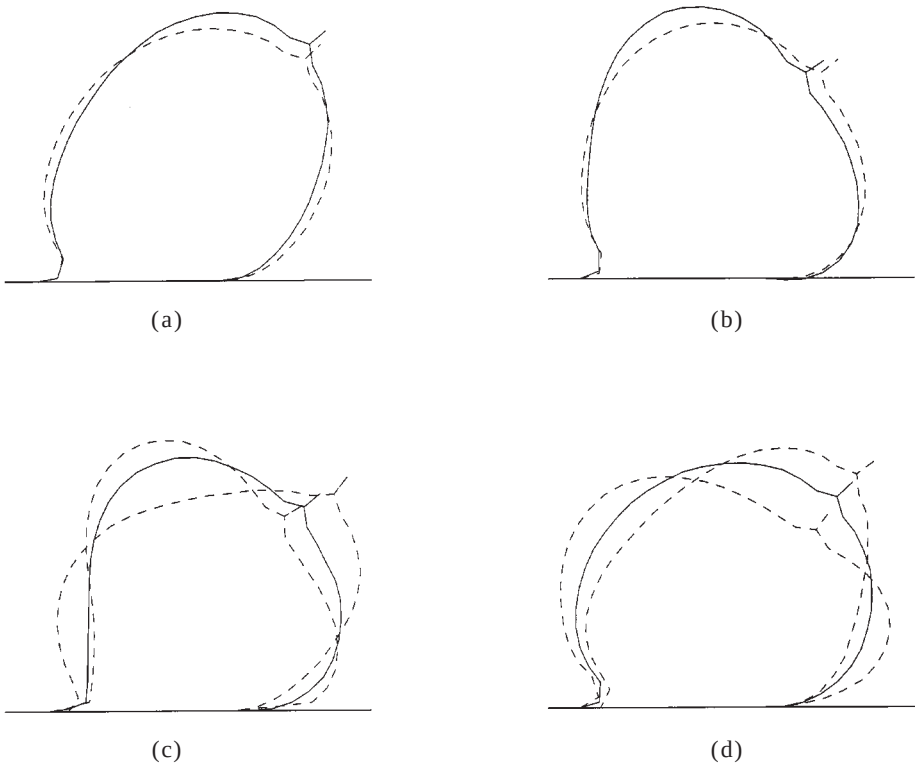

Figure 9. Cross sections of the modes in Figure 8 at the center (——) and at quarter lengths from the ends (– – –). (a) Mode 1; (b) mode 2; (c) mode 3; (d) mode 4.

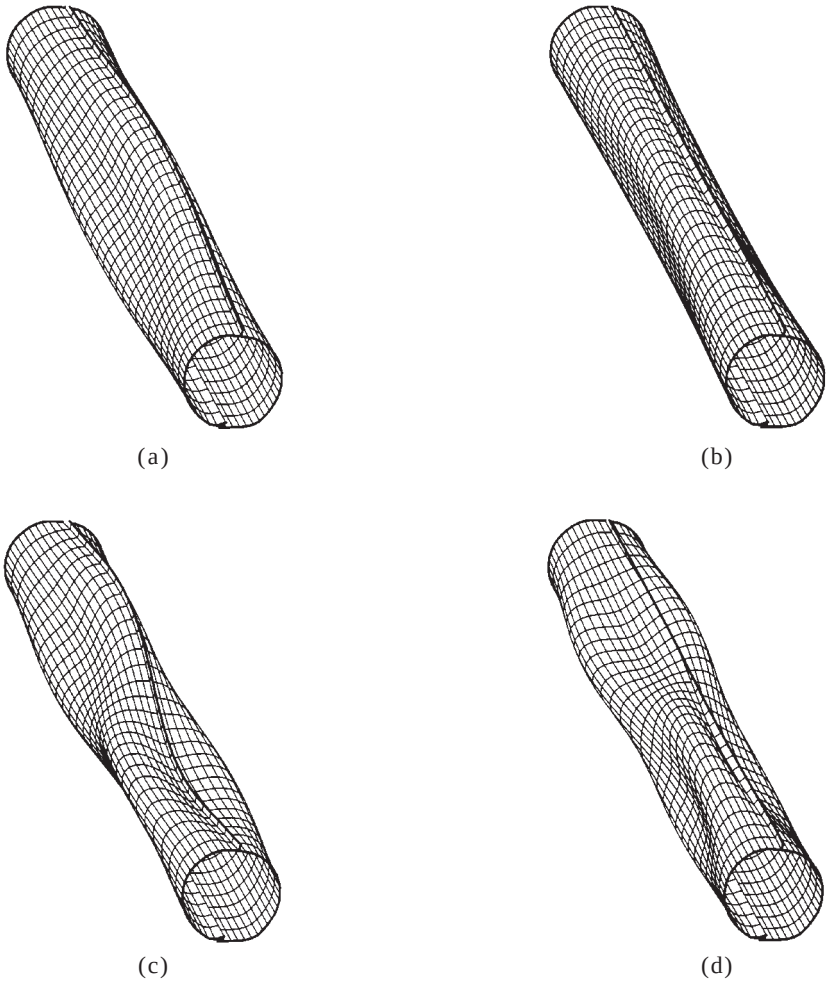

Figure 10. First four vibration modes without external water, for $p_{\text{int}} = 30$ kPa. (a) Mode 1; (b) mode 2; (c) mode 3; (d) mode 4.

Assuming time–harmonic motion at frequency ω_j, the amplitude $\xi_j(t)$ for each mode can be written as the real part of $\hat{\xi}_j \, e^{i\omega_j t}$ (no summation convention is used). The total velocity potential can be written as

$$\phi = \sum_j \xi_j(t)\phi_j(\mathbf{x}). \tag{5}$$

In the fluid domain, each velocity potential satisfies the Laplace equation

$$\nabla^2\phi_j = 0. \tag{6}$$

Assuming that the frequency of oscillation is high, the free-surface boundary condition reduces to the infinite-frequency limit of

$$\phi_j = 0. \tag{7}$$

In this case, no waves are generated by the free surface. The velocity potentials on S_b must satisfy the boundary condition that the velocity of the fluid on the dam is equal to that of the dam, i.e.

$$\frac{\partial \phi_j}{\partial n} = (V_n)_j = U_p \frac{\partial n_j}{\partial y} + i\omega_j n_j, \tag{8}$$

and those on the bottom surface S_h, the two side surfaces S_s, and the surface S_∞ must satisfy the no penetration condition

$$\frac{\partial \phi_j}{\partial n} = 0. \tag{9}$$

The velocity potentials are found using a boundary integral method. Following Hess and Smith [27], who were the first to develop the method to a practical stage, Green's theorem with an appropriate Green's function is used to reduce the problem to solving an integral equation on the fluid boundaries. We define a Green's function G consisting of a Rankine source minus its image above the free surface. We write

$$G(\mathbf{x}, \boldsymbol{\chi}) = \frac{1}{r} - \frac{1}{r'}, \tag{10}$$

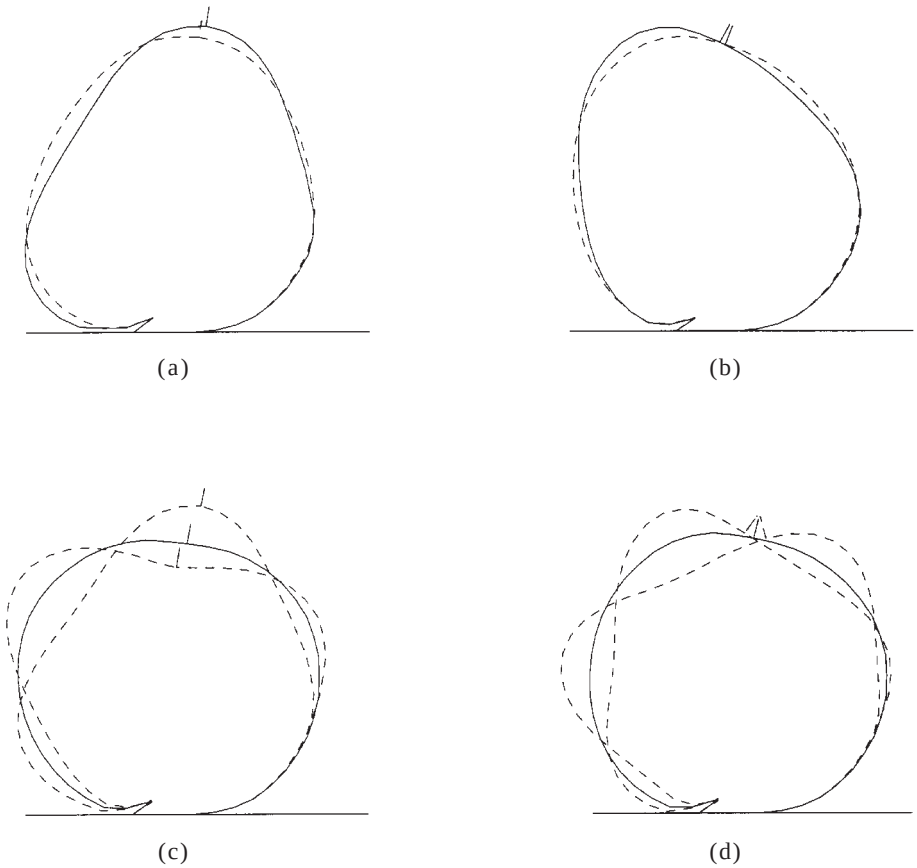

Figure 11. Cross sections of the modes in Figure 10 at the center (——) and at quarter lengths from the ends (– – –). (a) Mode 1; (b) mode 2; (c) mode 3; (d) mode 4.

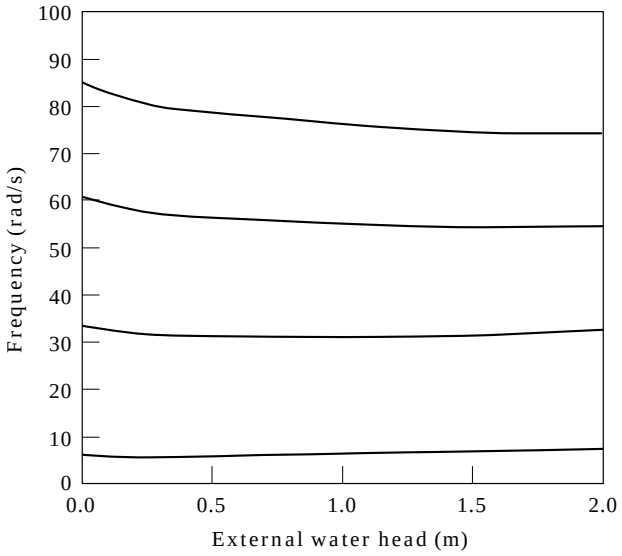

Figure 12. Variation of frequencies with external water head, for $p_{\text{int}} = 30$ kPa.

where $\mathbf{x} = (x, y, z)$ is the field point, $\boldsymbol{\chi} = (\chi, \eta, \zeta)$ is the source point, $r^2 = (x - \chi)^2 + (y - \eta)^2 + (z - \zeta)^2$ and $(r')^2 = (x - \chi)^2 + (y - \eta)^2 + (z + \zeta)^2$. Application of Green's second identity provides a Fredholm equation of the second kind for the values of the potential on the boundaries:

$$\phi_j(\mathbf{x}) + \int\int_{\partial D} \phi_j(\boldsymbol{\chi}) \frac{\partial G(\mathbf{x}, \boldsymbol{\chi})}{\partial n_\chi} \, \mathrm{d}S_\chi = \int\int_{\partial D} V_{n_j}(\boldsymbol{\chi}) G(\mathbf{x}, \boldsymbol{\chi}) \, \mathrm{d}S_\chi. \tag{11}$$

The fluid boundary ∂D consists of the body boundary S_b, the bottom S_h, two side surfaces S_s, and the surface S_∞. The free surface S_f is not discretized since the Green's function G satisfies the free-surface condition.

The integral equation (11) is solved numerically by replacing the body surface region S_b, the bottom S_h, and the surface S_∞ by an ensemble of quadrilateral elements of constant potential strength. In this study, 300 panels were used on S_b, 55 on each S_s, and 60 on S_∞. The results were found to be unaffected by the number of panels if more were used. Then the integral equation is satisfied at a set of collocation points (in this study the panel centroids are used), resulting in a linear system of equations for the unknown potential values. From the values of the velocity potentials on the body surface, the pressure on the dam and hence the added mass values may be obtained by using the standard definitions :

$$p_j = -\left[i\rho\omega_j\phi_j + \rho U_p \frac{\partial \phi_j}{\partial y} \right] \mathrm{e}^{i\omega_j t}. \tag{12}$$

Substituting the expression for pressure p_j in equation (4), we get

$$R_i = \rho \, \mathrm{e}^{i\omega_j t} \int\int_{S_b} \left[-i\omega_j\phi_j - U_p \frac{\partial \phi_j}{\partial y} \right] n_i \, \mathrm{d}S. \tag{13}$$

But R_i can be expressed as

$$R_i = -M_{ij}\ddot{\xi}_j - B_{ij}\dot{\xi}_j. \tag{14}$$

Replacing $\xi_j(t)$ by $\hat{\xi}_j\, e^{i\omega_j t}$, we get

$$R_i = [\omega_j^2 M_{ij} - i\omega_j B_{ij}]\hat{\xi}_j\, e^{i\omega_j t}. \tag{15}$$

By comparing equations (13) and (15), we get

$$(M_A)_{ij} - \frac{i}{\omega_j} B_{ij} = -\frac{i\rho}{\omega_j}\int\int_{S_b} \phi_j n_i \, dS - \frac{\rho U_p}{\omega_j^2}\int\int_{S_b} \frac{\partial \phi_j}{\partial y} n_i \, dS. \tag{16}$$

The change in pressure acts as additional inertia on the structure. Thus equation (2) now becomes

$$(M_g + M_A)\ddot{\xi} + B\dot{\xi} + K_g\xi = 0, \tag{17}$$

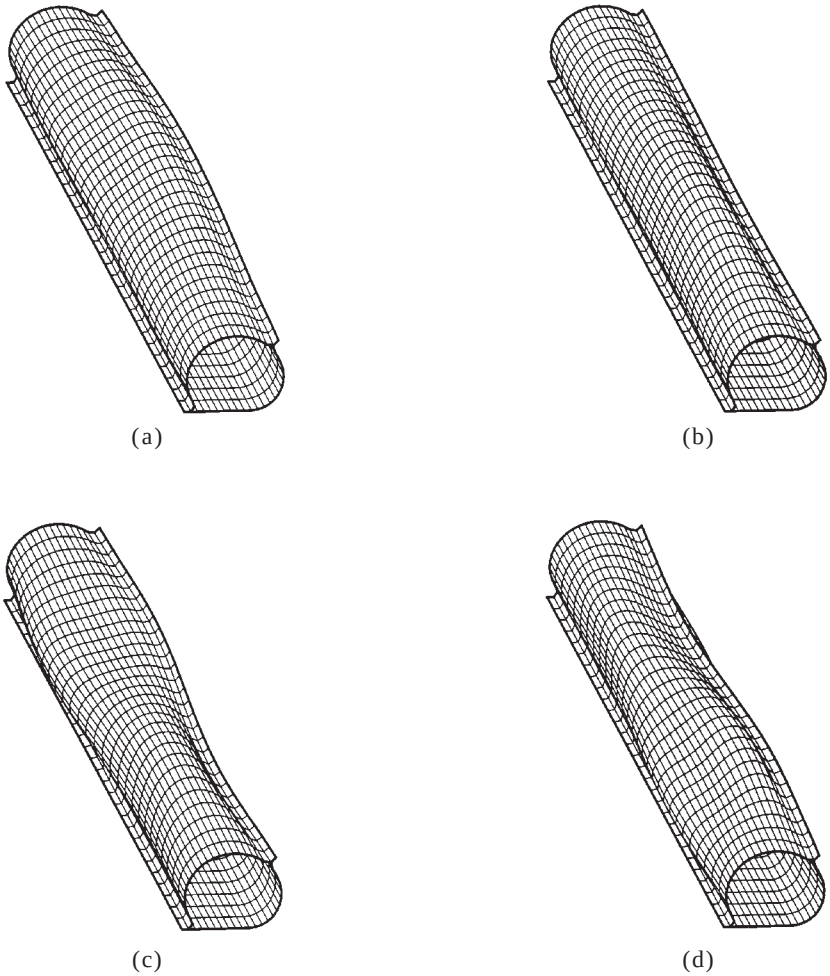

Figure 13. First four vibration modes with external water, for $p_{\text{int}} = 1$ kPa. (a) Mode 1; (b) mode 2; (c) mode 3; (d) mode 4.

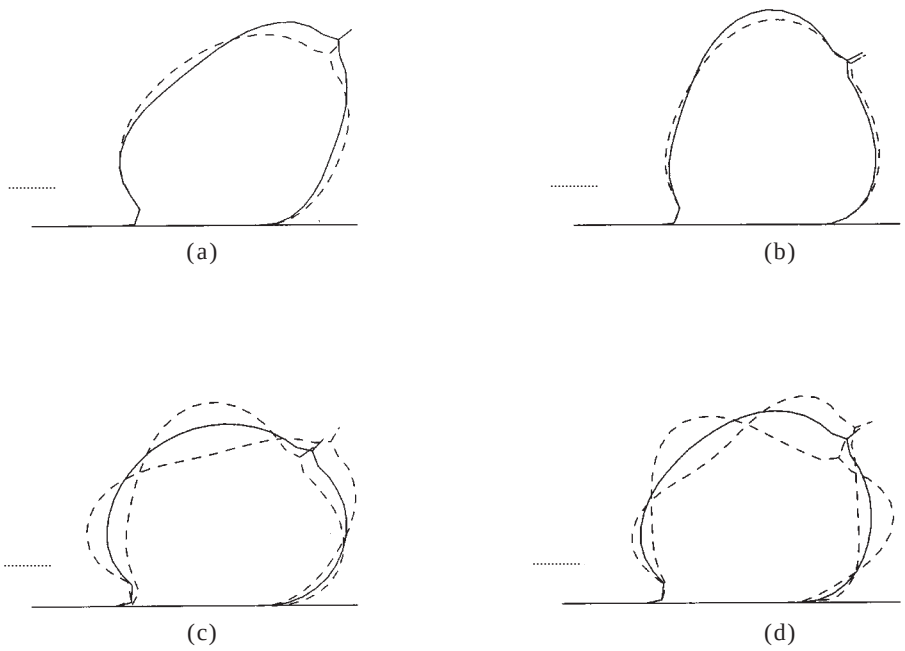

Figure 14. Cross sections of the modes in Figure 13 at the center (——) and at quarter lengths from the ends (– – –). (a) Mode 1; (b) mode 2; (c) mode 3; (d) mode 4.

where M_g and K_g are the generalized mass and stiffness matrices, respectively, of the dam at its equilibrium position, M_A is the added mass matrix of the structure, and B is the damping matrix of the structure. The matrices M_g and K_g are of dimension equal to the number of modes and obtained from ABAQUS. All the matrices in equation (17) are real and symmetric. In the present study the values of the damping coefficients were found to be small compared to the other values in equation (17). This should be expected since in the infinite-frequency limit, no waves are generated on the free surface and hence there is no wave damping. Replacing $\xi(t)$ by $\hat{\xi}\,e^{i\omega t}$ and neglecting damping, we can rewrite equation (17) as

$$[-\omega^2(M_g + M_A) + K_g]\hat{\xi} = 0. \tag{18}$$

Standard procedures can be utilized to solve the above eigenvalue problem to obtain the new natural frequencies and the eigenvectors. The eigenvectors can then be used along with the "dry" mode shapes to obtain the "wet" mode shapes.

4. LINEAR VIBRATIONS: RESULTS

4.1. PROCEDURE VALIDATION

To validate the procedure adopted to compute the natural frequencies of the structure with or without external water, two example cases are chosen. In the first example, a long circular cylindrical shell of length 80 m and radius 1 m is considered. First, the structure

is assumed to vibrate in air. The structure is assumed to be pinned at the ends and is restrained so as to allow vibrations only in a plane. The structure is modelled as a shell using 128 quadrilateral shell elements of the type S4R in ABAQUS, and the first four natural modes and frequencies of vibration are obtained. The length is much larger than the radius so that the numerical results should be close to the analytical results for a pinned-pinned beam. As is well known, the natural frequencies and mode shapes of a pinned-pinned beam are given by

$$\omega_n = \frac{n^2\pi^2}{L^2}\sqrt{EI/\mu}, \qquad y_n = \sin\left(\frac{n\pi x}{L}\right), \tag{19, 20}$$

where L is the length, EI is the bending stiffness, and μ is the mass per unit length of the beam.

The frequencies and mode shapes obtained numerically are in close agreement with those obtained from equations (19) and (20). The cylinder is then assumed to be completely

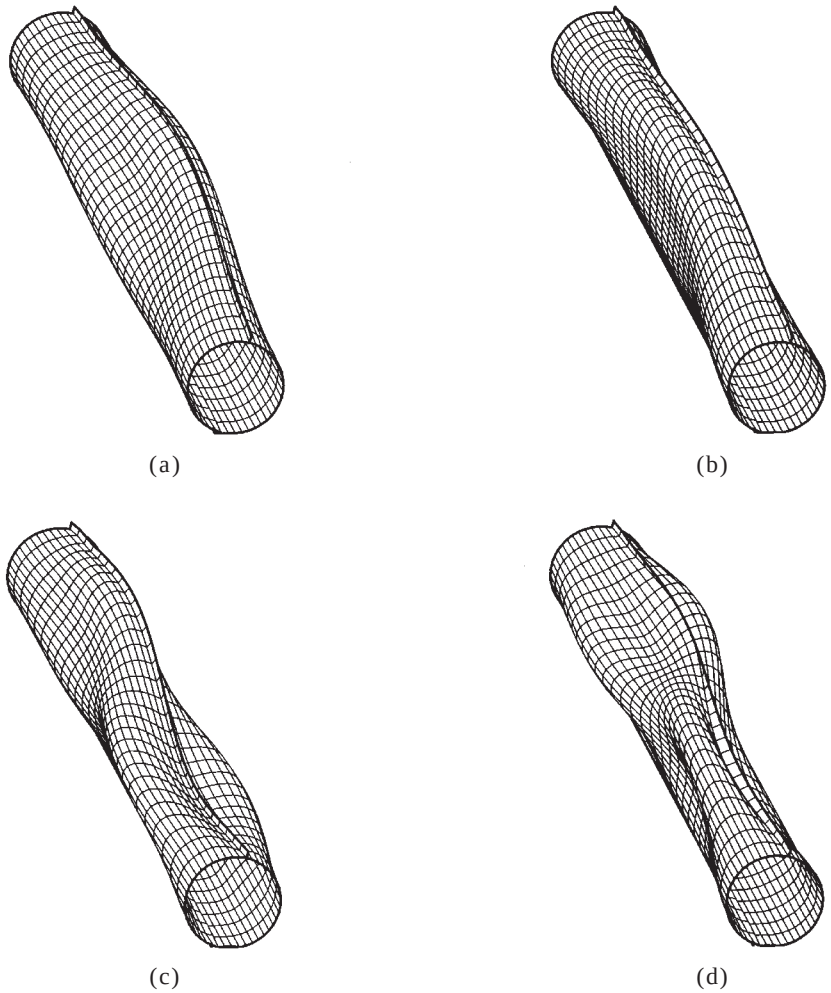

Figure 15. First four vibration modes with external water, for $p_{\text{int}} = 30$ kPa. (a) Mode 1; (b) mode 2; (c) mode 3; (d) mode 4.

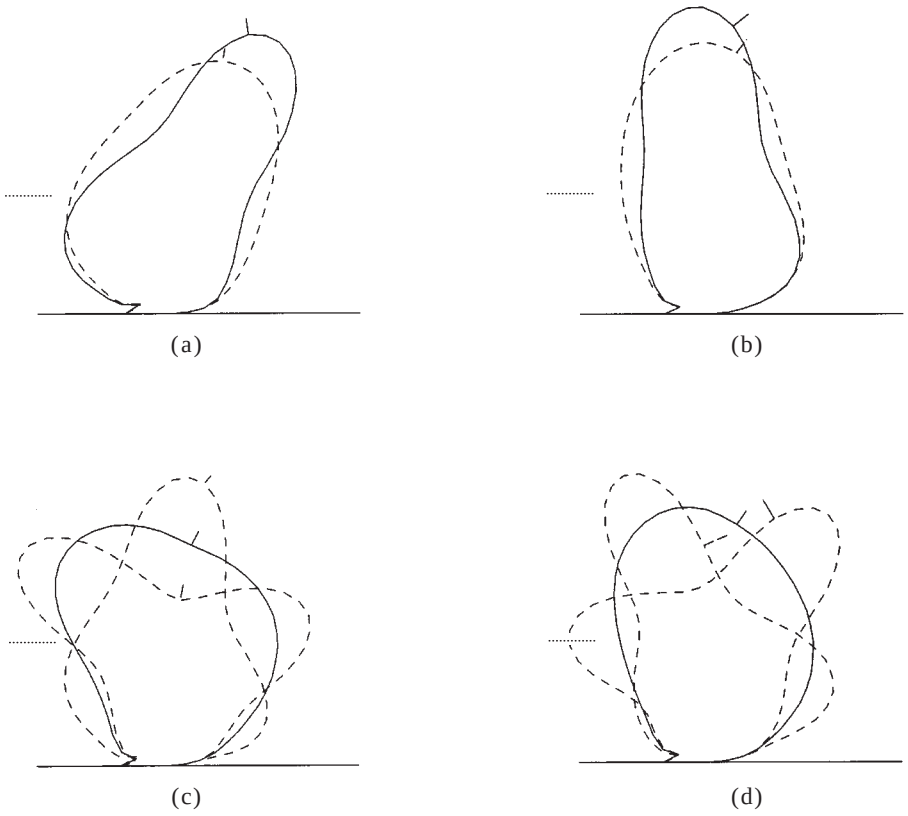

Figure 16. Cross sections of the modes in Figure 15 at the center (——) and at quarter lengths from the ends (– – –). (a) Mode 1; (b) mode 2; (c) mode 3; (d) mode 4.

submerged in water far away from the free surface so that free surface effects are not important. Because the length of the structure is much greater than its diameter, strip theory can be used to obtain the added mass coefficients for the first four mode shapes analytically. The vibration frequencies of the structure completely submerged in water are obtained by using Rayleigh's quotient:

$$\omega_n^2 = \frac{\int_L EI\left(\frac{\mathrm{d}^2 y_n}{\mathrm{d}x^2}\right)^2 \mathrm{d}x}{\int_L (\mu + m_A) y_n^2 \,\mathrm{d}x}, \tag{21}$$

TABLE 2

Natural frequencies (rad/s) of the dam with parallel flow, for $p_{int} = 1\ kPa$

Mode No.	Without water	With water	$U = 1{\cdot}0$ m/s	$U = 5{\cdot}0$ m/s
1	2·169	2·108	2·011	1·995
2	7·775	7·401	7·105	6·956
3	13·49	12·42	11·99	11·55
4	19·14	17·43	16·47	16·03

TABLE 3

Natural frequencies (rad/s) of the dam with parallel flow, for $p_{int} = 30\ kPa$

Mode No.	Without water	With water	$U = 1{\cdot}0$ m/s	$U = 5{\cdot}0$ m/s
1	5·943	6·311	6·241	6·188
2	33·32	30·87	29·98	29·56
3	60·67	53·82	52·61	51·98
4	84·91	74·12	72·81	70·32

where y_n is the mode shape and $m_A = \rho\pi R^2$, the sectional added mass of a 2-D cylinder. Here, ρ is the density of the water. The mode shapes y_n are given by equation (20).

Numerical values for the added mass coefficients and the natural frequencies are then obtained using the procedure discussed in section 3. A total of 256 panels (128 on the cylindrical surface and 64 each on the two ends of the cylinder) are used to discretize the body surface. The added mass values obtained numerically are in close agreement with those obtained by using strip theory and the numerical values of the natural frequencies closely match those obtained from equation (21).

In the second example, the procedure is applied to compute the first four vibration modes and frequencies of the double-anchored inflatable dam which was considered in reference [14]. The vibration frequencies and mode shapes of the dam both in the presence and absence of external water are computed. The vibration frequencies and mode shapes obtained are in close agreement with those obtained in reference [14]. The maximum difference in the first four frequencies is 10% without water and 11% with water.

4.2. NUMERICAL RESULTS

4.2.1. *Without external water*

Consider dams that are not impounding water. For the vibration analysis the dam is clamped at the ends once the equilibrium shape is obtained. Small three-dimensional vibrations are then considered about the equilibrium configuration.

Fifteen modes are used . Results for the first four vibration frequencies and mode shapes are presented in Figures 7–11. Figure 7 shows the variation of the frequencies with internal pressure for the first four vibration modes, and Table 1 lists the corresponding frequencies for $p_{\text{int}} = 1$ kPa and 30 kPa. The slopes of the curves in Figure 7 decrease as the internal pressure increases. The vibration frequencies increase with the internal pressure, as one would expect. The squares of the frequencies vary almost linearly with the internal pressure. Figures 8 and 10 depict the first four vibration mode shapes for internal pressures of 1 kPa and 30 kPa, respectively. The first and second modes are symmetric and the third and fourth modes are anti-symmetric longitudinally. The corresponding profiles of the central cross-section for these modes (solid curves) and the cross-sections at a distance of one-quarter length from each end (dashed curves) are illustrated in Figures 9 and 11 for internal pressures of 1 kPa and 30 kPa, respectively. For the modes that are symmetric longitudinally, the two dashed curves are identical.

4.2.2. *With external water*

For the case of the dam impounding water on one side, the dam is clamped along the equilibrium cross-sections at its two ends, and then water is applied on the anchored side with a height less than the "dry" equilibrium height. The new equilibrium configuration is obtained and small vibrations of the dam about this equilibrium shape are analyzed.

The results are presented in Figures 12–16. Figure 12 depicts the variation of the first four frequencies with the external water head, for an internal pressure $p_{int} = 30$ kPa. The frequencies tend to decrease first and then increase as the external water head increases. The frequencies for the higher modes (modes 3 and 4) show more variation compared to those for the lower modes (modes 1 and 2). Table 1 compares the vibration frequencies of the dam with no external water to those for the dam in the presence of external hydrostatic water, for $p_{int} = 1$ kPa and 30 kPa. The external water head is 0·5 m and 1·5 m, respectively.

The corresponding first four modes are depicted in Figures 13 and 15, respectively. The frequencies of the structure in the presence of water are lower than those in the absence of water by a maximum of 11·3% in Table 1. The first and second modes are symmetric and the third and fourth modes are anti-symmetric longitudinally. Figures 14 and 16 show the cross-sectional behavior of the modes at the half-length (solid curves) and quarter-lengths (dashed curves) from each end of the dam for internal pressures of 1 kPa and 30 kPa, respectively. In Figures 14 and 16, the horizontal line at the left of the dam indicates the water height. For the first two modes the two dashed curves are identical.

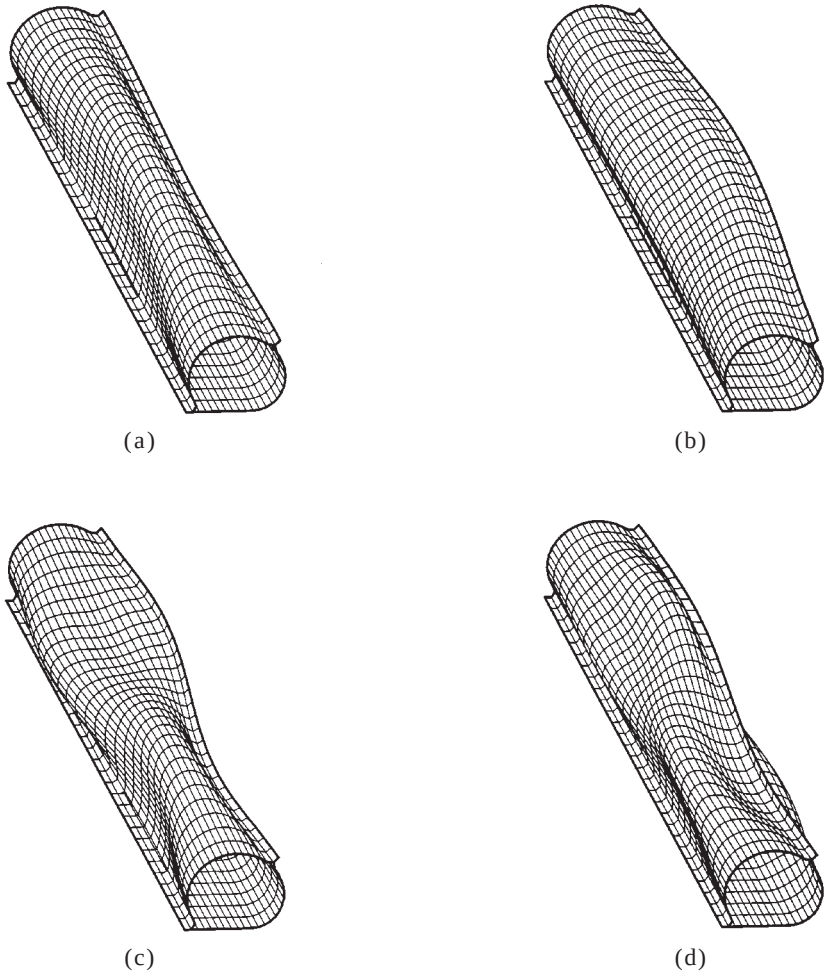

Figure 17. First four vibration modes with parallel flow of 5 m/s, for $p_{int} = 1$ kPa. (a) Mode 1; (b) mode 2; (c) mode 3; (d) mode 4.

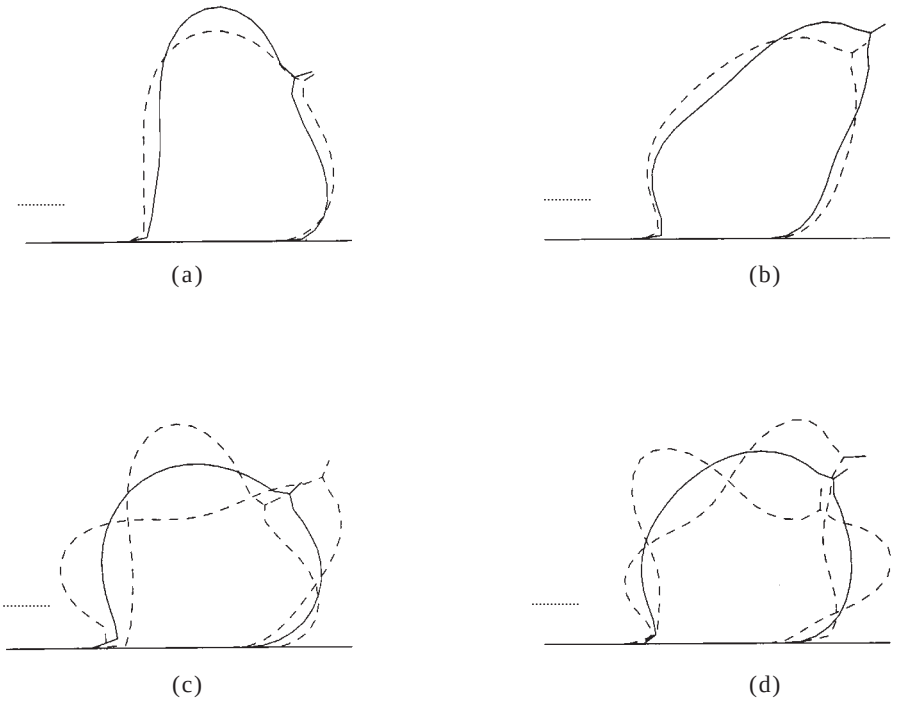

Figure 18. Cross sections of the modes in Figure 17 at the center (——) and at quarter-lengths from the ends (– – –). (a) Mode 1; (b) mode 2; (c) mode 3; (d) mode 4.

The cross-sectional behavior of the dam in the presence of external water, at half-length and quarter-lengths from the ends, is similar to that of the dam in the absence of water for both the internal pressures.

4.2.3. *With parallel flowing water*

The case of external water flowing parallel to the dam is considered. This situation may occur for a dam deployed along a river. In this case, the dam is clamped along the equilibrium cross-sections at its two ends, and then parallel flowing water is applied on the anchored side with the same height as that in the case of hydrostatic water (section 4.2.1). The equilibrium configuration is the same as that obtained for the case of the dam impounding hydrostatic water. Small vibrations of the dam about this equilibrium shape are analyzed. The direction of the flow is from the nearer end to the farther end along the length of the dam in Figures 17 and 19. The flow introduces hydrodynamic pressure and thus the boundary conditions on the structure change due to the fluid–structure interaction.

The vibration analysis was performed for internal pressures of 1 kPa and 30 kPa, as in the earlier cases. Flow velocities of 1 m/s and 5 m/s were considered. The natural frequencies and the corresponding mode shapes were obtained using the procedures described in section 3.2. The frequencies of vibration for the dam with internal pressures

of 1 kPa and 30 kPa are presented in Tables 2 and 3, respectively, and they are reduced by a maximum of 16·4% and 17·2%, respectively.

For the dam with internal pressure of 1 kPa, Figures 17 and 18 depict the mode shapes for a flow velocity of 5 m/s. Figure 18 illustrates the corresponding cross-sectional shapes at the center and quarter lengths from the ends of the dam. Figures 19 and 20 correspond to an internal pressure of 30 kPa and the same flow velocity. The mode shapes for a flow velocity of 1 m/s are similar to those shown.

5. CONCLUDING REMARKS

Vibrations of double-anchor inflatable dams impounding water on one side have been investigated previously [2, 14]. Most of the dams built today are single-anchored and have fins to facilitate smooth overflow. Therefore this type of dam was modelled here. The dam was assumed to rest on a rigid foundation.

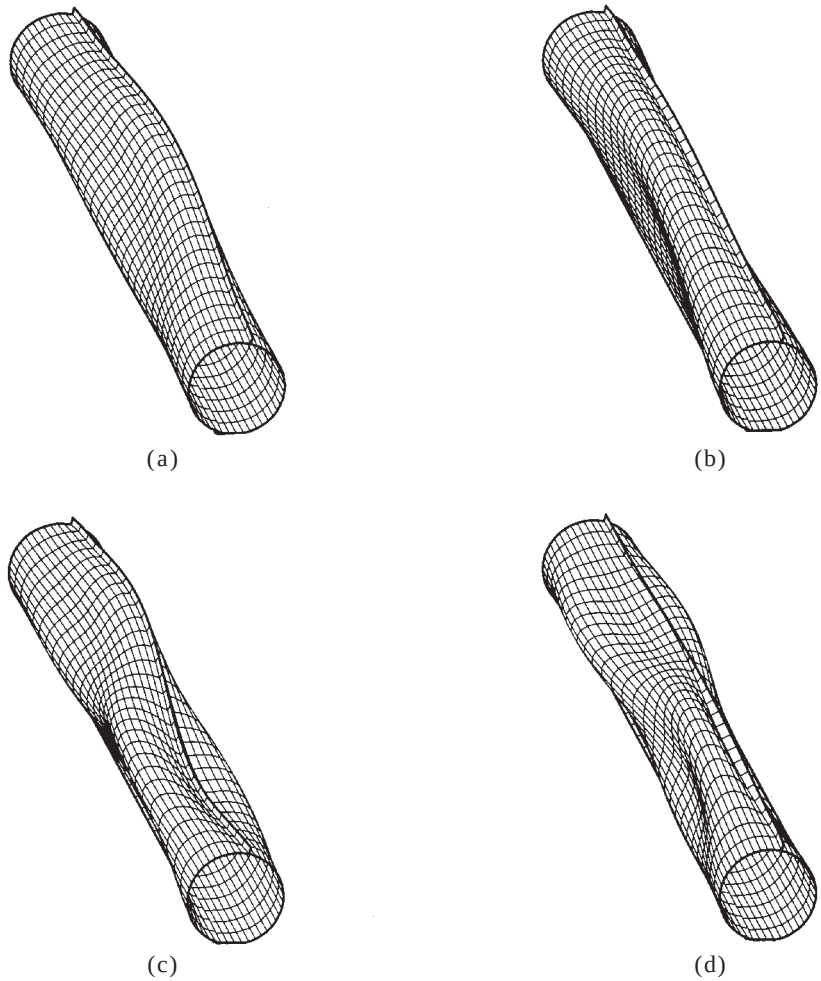

Figure 19. First four vibration modes with parallel flow of 5 m/s, for $p_{int} = 30$ kPa. (a) Mode 1; (b) mode 2; (c) mode 3; (d) mode 4.

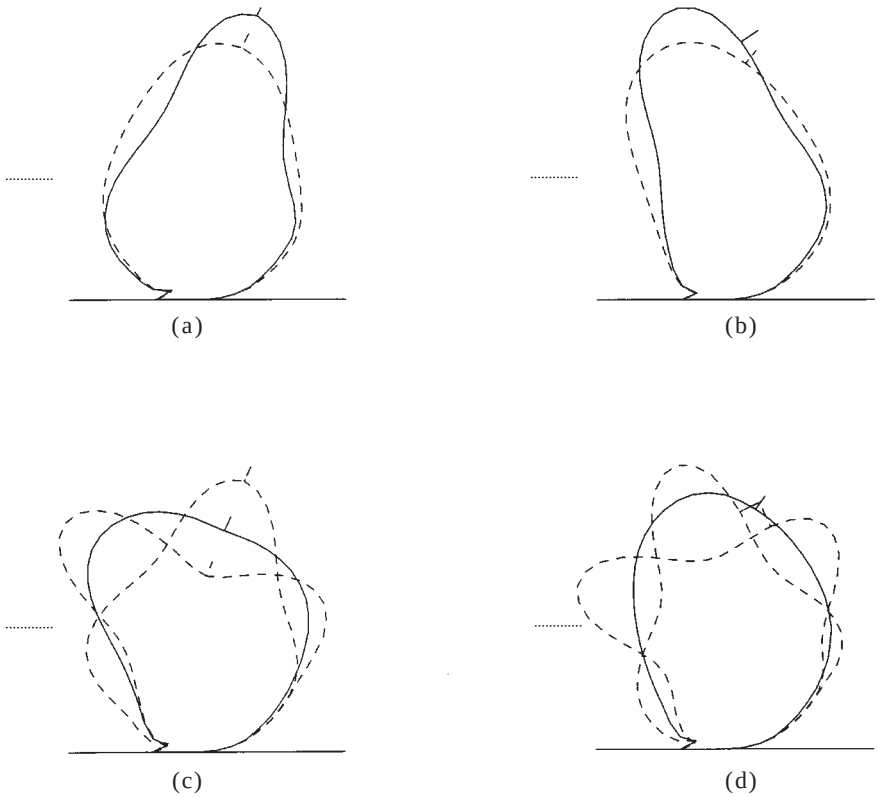

Figure 20. Cross sections of the modes in Figure 19 at the center (——) and at quarter-lengths from the ends (– – –). (a) Mode 1; (b) mode 2; (c) mode 3; (d) mode 4.

First the equilibrium shape was determined. Then small vibrations of the dam about the equilibrium configuration were studied. The lowest four vibration frequencies and corresponding mode shapes were computed. The frequencies are in the same range as those found for a double-anchor inflatable dam [14]. The case of a dam without external water was treated for comparison purposes.

In the vibration results, the length of the dam was about ten times its height, and the ends were fixed. The height of the external water was less than one-half the height of the dam. Some of the mode shapes are symmetric in the longitudinal direction and the others are anti-symmetric.

The rigid foundation tends to increase the frequencies. The presence of impounded water tends to lower the frequencies, as one would expect. The vibration frequencies of the dam impounding water were compared to those of the dam without external water. The vibration frequencies listed in Table 1 are reduced by up to 11·3% when the external water is present.

Finally, the case of the dam impounding water flowing parallel to the dam is considered. The flow pushes the dam further to the other side. The hydrodynamic pressure due to the external parallel flow results in added inertia (i.e. added mass) which tends to reduce the vibration frequencies of the dam. The reduction depends upon the internal pressure, external water head, and flow velocity. In this study, vibration results of the dam

corresponding to flow velocities of 1 m/s and 5 m/s are presented. In the two cases considered, the frequencies reduce by a maximum of 17·2% as compared to the frequencies of the dam without any external water. The changes in the equilibrium configuration and other factors such as added mass cause the changes in the mode shapes and frequencies of the dam.

ACKNOWLEDGMENT

This research was supported by the National Science Foundation under Grant No. CMS-9422248.

REFERENCES

1. N. M. Imbertson 1960 *Journal of the American Water Works Association* **52**, 1373–1378. Automatic rubber diversion dam in the Los Angeles River.
2. J.-C. Hsieh and R. H. Plaut 1990 *Acta Mechanica* **85**, 207–220. Free vibrations of inflatable dams.
3. J. Mika 1981 *Archiwum Hydrotechniki* **28**, 569–583. General computing model of hydrotechnical flexible closures (in Polish).
4. D. S. Wakefield 1987 in *Proceedings of the International Conference on the Design and Construction of Non-Conventional Structures*, B. H. V. Topping, ed., **2**, 75–80. Edinburgh: Civil-Comp Press. Practical numerical modelling of complex structures.
5. M. Abdulrazzak, A. Sorman and A. Alhames 1988 in *Artificial Recharge of Ground Water*, A. I. Johnson and D. J. Finlayson, ed., 602–611. New York: ASCE. Techniques of artificial recharge from an ephemeral Wadi channel under extreme arid conditions.
6. C. T. F. Ross 1988 in *Finite Element Analysis of Thin-Walled Structures*, J. W. Bull, ed., 93–132. London: Elsevier Science. The analysis of thin-walled membrane structures using finite elements.
7. T. Kahl and S. Ruell 1989 in *Waterpower* '89, A. J. Eberhardt, ed., **1**, 447–456. New York: ASCE. Flashboard alternatives including rubber dams.
8. G. Bolzon, B. A. Schrefler and R. Vitaliani 1990 in *Computational Mechanics of Nonlinear Response of Shells*, W. Krätzig and E. Oñate, ed., 348–377. Berlin: Springer. Finite element analysis of rubber membranes.
9. C. R. Nelson 1992 *Public Works* **123**, 56–57. Conserving local water resources brings drought relief.
10. A. M. Al-Brahim 1994 *European Earthquake Engineering* **8**, 31–37. Free vibration of membrane dams.
11. T. A. Economides and D. A. Walker 1994 in *Fundamentals and Advancements in Hydraulic Measurements and Experimentation*, C. A. Pugh, ed., 500–506. New York: ASCE. Non-intrusive experimental setup for inflatable dam models.
12. M. R. Markus, C. A. Thompson and M. Ulukaya 1994 in *Proceedings of the International Symposium on Artificial Recharge of Ground Water*, *II*, A. I. Johnson and R. D. G. Pyne, ed., 120–128. New York: ASCE. Enhanced artificial recharge utilizing inflatable rubber dams.
13. M. R. Markus, C. A. Thompson and M. Ulukaya 1995 *Water Engineering and Management* **142**, 37–40. Aquifer recharge enhanced with rubber dam installations.
14. C. M. Dakshina Moorthy, J. N. Reddy and R. H. Plaut 1995 *Thin-Walled Structures* **21**, 291–306. Three-dimensional vibrations of inflatable dams.
15. J. A. Higgs 1996 *Memorandum Report*, *Water Resources Research Laboratory*, *Bureau of Reclamation*, *Denver*, *Colorado*. Friant Dam spillway rehabilitation: hydraulic model study.
16. C. H. Sehgal 1996 *Journal of Hydraulic Engineering* **122**, 155–165. Design guidelines for spillway gates.
17. P.-H. Wu and R. H. Plaut 1996 *Thin-Walled Structures* **26**, 241–259. Analysis of the vibration of inflatable dams under overflow conditions.
18. P. W. M. Tam 1997 *Journal of Irrigation and Drainage Engineering* **123**, 73–78. Use of rubber dams for flood mitigation in Hong Kong.
19. V. I. Weingarten, S. F. Masri and M. Lashkari 1973 in *Hydromechanically Loaded Shells*, R. Szilard, ed., 591–601. Honolulu: University Press of Hawaii. Free vibrations of a partially submerged cylindrical shell.

20. C. T. F. Ross 1990 *Pressure Vessels Under External Pressure*: *Statics and Dynamics*. London: Elsevier Science.
21. A. Ergin, W. G. Price, R. Randall and P. Temarel 1992 *Journal of Ship Research* **36**, 154–167. Dynamic characteristics of a submerged, flexible cylinder vibrating in finite water depths.
22. J. A. Giordano and G. H. Koopmann 1995 *Journal of the Acoustical Society of America* **98**, 363–372. State space boundary element—finite element coupling for fluid–structure interaction analysis.
23. T. Hamamoto, T. Hayashi and K.-I. Fujita 1996 in *Proceedings of the Sixth International Offshore and Polar Engineering Conference*, J. S. Chung *et al*., ed., **I**, 362–369. Golden, CO: International Society of Offshore and Polar Engineers. 3D BEM-FEM coupled hydroelastic analysis of irregular shaped, module linked large floating structures.
24. D. E. Beskos 1997 *Applied Mechanics Reviews* **50**, 149–197. Boundary element methods in dynamic analysis: part II (1986–1996).
25. ABAQUS 1994 *Theory Manual*, Vol. I, Version 5.4. Pawtucket, RI: Hibbitt, Karlsson & Sorensen, Inc.
26. J. N. Newman 1994 *Applied Ocean Research* **16**, 47–59. Wave effects on deformable bodies.
27. J. L. Hess and A. M. Smith 1964 *Journal of Ship Research* **8**, 22–44. Calculation of non-lifting potential flow about arbitrary three-dimensional bodies.